# AIR-WAKE PREDICTION BASED AIR-VEHICLE RECOVERY AIDS

**M R Belmont,** University of Exeter, UK. **J Christmas,** University of Exeter, UK. **B Ferrier**, Hoffman Engineering, USA. **J D Duncan,** UK Ministry of Defence (retired) and **J Duncan**, Morsons Ltd UK.

(Reference No: IJME682, DOI No: 10.5750/ijme.v163iA3.802)

KEY DATES: Submitted: 23/11/20; Final acceptance: 12/08/21; Published 16/11/21

**SUMMARY**

This report demonstrates the capability of the forward prediction of the properties of the arriving wind at a vessel for time intervals adequate to significantly aid in the recovery of a wide range of air vehicles onto vessels. For craft with flight decks sited in the fore part of the vessel it is adequate to simply predict the arriving wind. For the more difficult task of recovery to stern areas behind superstructure it is also necessary to predict either the explicit properties of the turbulent air-wake or else to predict some quality measure for the aid of recovery under the prevailing conditions. The approach is able to relate the trends in the short-term statistical properties of fluctuating airflow over the flight deck to the trends in the predicted arriving wind.

## NOMENCLATURE

| | |
|---|---|
| $a_i$ | *The $i^{th}$ coefficient of the space/time wind evolution model.* |
| $n$ | *Summation index; of $N$ in total.* |
| $s(t)$ | *Advection distance.* |
| $t$ | *Time.* |
| $t_n$ | *The $n^{th}$ discrete time step number.* |
| $V$ | *Maximum wind velocity component measured along the LiDAR beam.* |
| $x$ | *Space coordinate along maximum wind velocity component measured along the LiDAR beam.* |
| $x_0$ | *The maximum value of the x coordinate.* |
| $\lambda$, $\tau$ | *Integration variables.* |

## 1. INTRODUCTION

The present approach to operating both fixed and rotary wing manned and unmanned aircraft from ships is based around measuring the short-term statistics of the prevailing wind speed and direction into the vessel and comparing this against a designated safe limit. This measure is frequently termed a SHOL which collectively specifies the range of allowed wind conditions and approach directions for recovery of a given air vehicle onto a specific vessel type. A fundamental difficulty with this statistical approach is that to achieve an acceptably low level of risk the prevailing values must be several standard deviations less than the safe tolerable maximum. This is to avoid the low but finite probability of extreme wind fluctuations. The result is either a very conservative approach that dramatically reduces the operational capability, and hence value for money, and or increases risk. For manned aircraft one alternative is to limit operations to the most experienced pilots which has its own consequences.

The increasing move towards unmanned air-vehicles (UAVs) for a wide range of maritime roles in both the civil and military sectors aggravates this situation. This is because not only is it difficult to incorporate the skill of a manned pilot into the UAV flight controller but also in general UAVs are substantially smaller than their manned counterparts and have less penetration in chaotic airflows. Particularly challenging issues during UAV recovery are the combination of the highly disturbed air-wake produced by the vessel's superstructure and the confined spaces typically available for recovery. Many custom recovery technologies have been developed to attempt to address this problem, ranging from nets to the line capture system used for the Boeing ScanEagle. However, these approaches are very difficult to operate in highly disturbed airflows without endangering the UAV. The situation is so difficult that in some first-generation applications operated by navies the UAV is required to ditch in the sea for subsequent small boat recovery which is clearly not a sustainable long-term strategy. Clearly the recovery problem becomes rapidly more demanding the higher the prevailing wind speed.

Fortunately, the very fluctuations in typical winds that make the statistical approach to recovery problematic can be turned to advantage if the quieter periods (quiescent periods) inevitably present (where the wind is significantly less intense than the mean) could actually be reliably predicted in advance. It is not sufficient to merely measure the wind at the vessel bow to achieve this because recovery of the UAV from its safe loitering position off from the vessel takes a significant time. However, the technology of long-range Doppler LiDAR, (Banakh et al, 1997, Drobin et al 2004, Davies et al 2004, O'Connor et al 2010, Liu et al 2019), has made such prediction possible, with the available predict ahead times being significantly longer than needed for reliable identification of the quiescent periods.

This report examines the requirements of a Doppler LiDAR based aircraft recovery aid and describes field trials conducted to explore such a system. This new technique both considerably extends the wind speeds for recovery but does so with the increased safety stemming from a deterministic rather than statistical approach.

The work presented here represents one aspect of the proposed new generation predictive launch and recovery aids. These involve making short term deterministic estimates of the safest period in which to execute a potentially hazardous operation.

The other main environmental factor to air wake is the deterministic prediction of wave induced vessel motion. Both deterministic air wake and wave prediction share the same underlying elements:

(i) Make measurements of the wind or wave system several km from the vessel.

(ii) Estimate the form of the wind or wave system when it has propagated to the vessel location.

(iii) Predict the time interval when the environmental factors will have minimal impact on the operation of interest. These are so called quiescent periods.

## 2. MAIN BODY

### 2.1 AIR-WAKE PREDICTION BASED RECOVERY AID CONCEPT

Figure 1 shows schematically the basis of an air-wake quiescent period prediction system for aiding ship born aircraft recovery. As is frequently the case in naval vessels the region designated for operating air-vehicles is at the stern behind the aft superstructure making recoveries subject to a considerably chaotic air-wake.

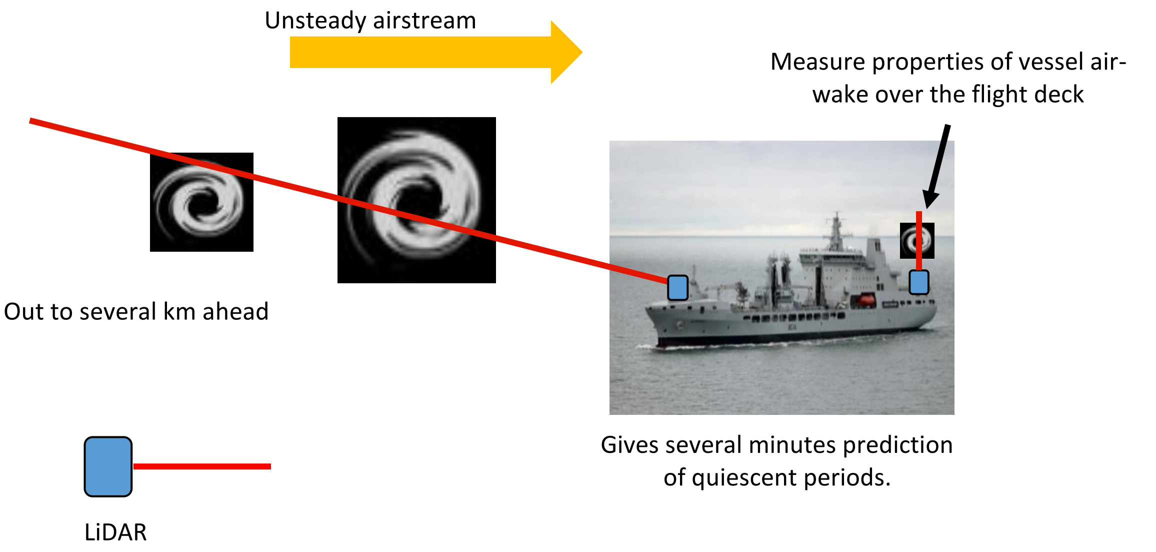


Figure 1. A schematic for an Air-wake Quiescent Prediction system for use as an aircraft recovery aid based around a long-range Doppler LiDAR.

 ©2021: The Royal Institution of Naval Architects

The Doppler LiDAR system projects an infrared laser beam (required to be eye-safe) out to several km and measures the component of the airflow along the beam line via Doppler shifts introduced during scattering by atmospheric aerosols. In order to also assess the cross-beam component of the wind the LiDAR measurement beam is scanned horizontally in a fan of individual single beam scans.

Various sea trials have been conducted to explore this approach (described in detail in section 4), supported by the UK Ministry of Defence. A typical resulting two-dimensional slice of wind speed values and directions determined from the long range scanning Doppler LiDAR measurements is shown in Figure 2. This figure illustrates the spatial details of the smaller scale wind gust structures present.

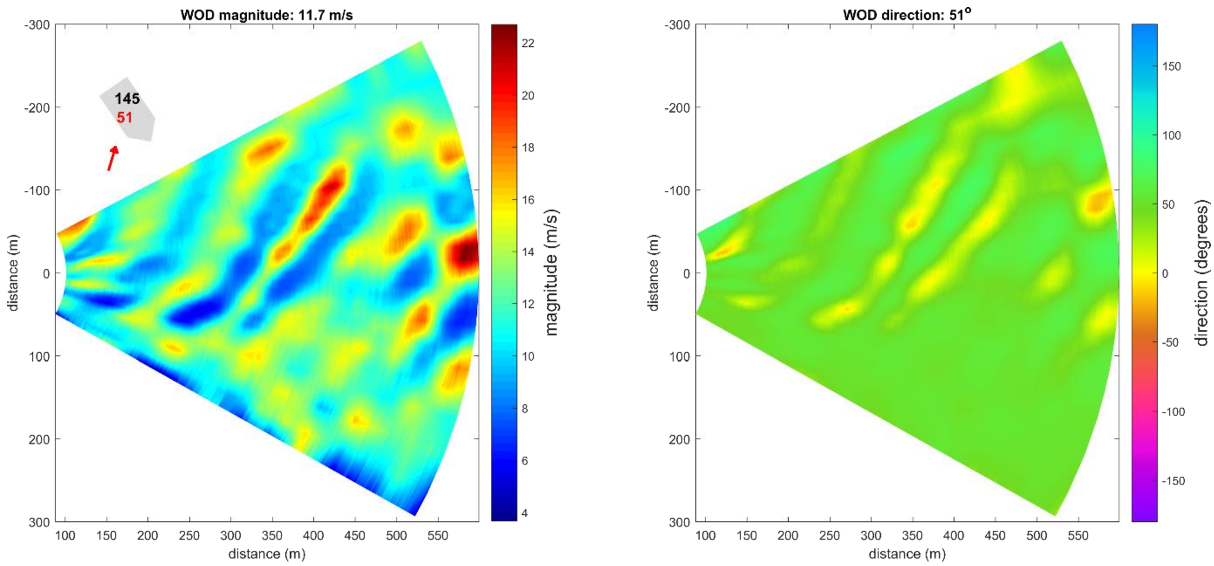


Figure 2. A typical two-dimensional slice of wind velocity and direction values obtained using long range Doppler LiDAR. The small red arrow denotes the mean wind direction relative to the vessel.

## 2.2 AIR-WAKE PROPAGATION AND PREDICTION

The predict-ahead time aspect of an air-wake quiescence prediction system arises from the time taken for the remotely measured wind system to propagate to the vessel. In principle the Doppler LiDAR data could be used as the input to a computational fluid dynamics (CFD) software system to predict not only the arriving airflow at a vessel but also properties of the subsequent air-wake over the ship induced by the arriving wind.

As will be discussed in subsequently while this CFD approach is valuable in creating off-line key functional elements of the system it cannot be used to make the actual real time predictions themselves CFD due to the very long computational times required. A great benefit of CFD is that it can describe three-dimensional flow. However even if the approach was computationally viable the time needed to acquire three-dimensional LiDAR data would render the approach unrealistic.

Hence an advection model of some nature is required to estimate the propagation of the measured wind profile up to the vessel. For a practical system even substantial errors in such propagation can be tolerated because the errors tend to scale with absolute wind speed allowing reliable confidence bounds can be established to guide a user's reliance on the predictions.

The simplest approach is spatially averaged advection (sometimes called "magic carpeting") which involves first measuring the spatial profile at time $t_0$ of the velocity component directed towards the vessel, $V(x, t_0)$, from the vessel out to the maximum measurement range. Then the spatial average, $\bar{V}_x$, of this quantity is determined, $\bar{V} = \left\langle V\left(x,t_0\right)\right\rangle_x$. The whole measured velocity profile is then simply advected bodily towards the vessel.

For short prediction times the local mean wind does not evolve significantly hence this very simple method is adequate for the recovery of even moderate sized rotorcraft where 10 seconds or less prediction time is required. Where longer prediction times are needed for example in the rapid recovery of a swarm of small UAVs, or for larger aircraft such as Merlin it is useful to explore other methods. Such recovery times were supplied by a combination of the Royal Navy and air vehicle manufacturers, (e.g., Agusta Westland for Merlin).

The spatial mean wind technique does not allow for temporal evolution in the local mean velocity component as the wind system propagates towards the vessel. A more sophisticated approach is the time evolving advection technique which involves making a spatio-temporal model of the spatially local mean value of, $V(x,t)$, of the type produced by empirical mode decomposition techniques, (Huang 1971).

Such a time dependent local advection velocity model then allows the local mean advection velocity, $V(x,t)$, to evolve over the propagation time. This can be accomplished using, $N$, successive LiDAR scans taken at times, $t_n$, $0 \le n \le N$, to build a short term least-squares fit model of the local mean value of, $V(x,t)$, in the variables, $x$, and, $t$. For this process to be reliable it is necessary to measure out to ranges, $x_{\max}$, well beyond the parts of the profile that will propagate to the vessel during the predict ahead time, $t_p$. In effect this scheme is estimating the, $x$, component of flow structures in the prevailing wind up to size scale, $x_{\max}$.

The analysis of this more sophisticated advection model is undertaken in section A1 in the appendix. A linear spatio-temporal model for the local velocity results in the expression given in equation 1 for the forward facing, $x(t)$, coordinate at time, $t$, of a point which started at time, $t=0$, at a location, $x_0$, measured out from the vessel along the LiDAR beam (in the direction of maximum wind velocity):

$$x(t) = x_0 - \frac{\sqrt{2\pi}\left(a_0 a_3 - a_1 a_2\right)}{2\left(-a_3\right)^{\frac{3}{2}}} \times \left\{ e^{\frac{-\left(a_1 + a_3 t\right)^2}{2a_3}} erf\left(\frac{\left(a_1 + a_3 t\right)}{\sqrt{-2a_3}}\right) - e^{-\frac{a_1^2}{2a_3}} erf\left(\frac{a_1}{\sqrt{-2a_3}}\right) \right\} \quad\text{.................}1$$

where the, $a_i$, are coefficients in a first order spatio-temporal model for, $V(x,t)$. If higher order corrections are required, then a perturbation approach is the natural route. The analysis required for a quadratic spatio-temporal local velocity model is developed in section A2 of appendix I.

This spatio-temporal modelling approach to the local velocity allows more precise prediction of the advection process and is computationally inexpensive. Consequently, unlike a CFD based methodology it can deliver the required real time operation of the prediction system to predict ahead times of several hundreds of seconds.

Further refinements involve involving fans of LiDAR scans in the actual prediction process instead of merely measurements along the beam line. Such data describes two dimensional slices through the wind structure and makes it possible to lift the assumption that the wind direction is constant over the prediction timescale. However as will be shown in section 4 the simpler one-dimensional advection methods have proved adequate in practice.

Apart from the CFD approach, which as stated is not possible for real time prediction, all the above techniques neglect non-linearities that cause the very local shape of the turbulent eddies within the profile to evolve (the so-called turbulent cascade process). Such local changes should not be confused with changes in the local mean velocity of the profile shape as modelled in the time evolving advection method. This implicit assumption that the local eddy shape is conserved during short term fluid transport was considered by G.I.Taylor and forms the basis of his well-known frozen turbulence hypothesis, (Taylor 1938, Frisch et al 1995, Sreenivason et al 1996). Extensive subsequent research has shown that provided the velocity fluctuations within the turbulent eddies are no greater than approximately half the local mean velocity then this hypothesis holds. The details of the measured turbulent structures (the gusts) can thus be simply advected with negligible change in shape. This provides a strong justification for the local advection-based approaches to prediction employed here and explains their success.

### 2.3 PREDICTING THE VESSEL AIR-WAKE PROPERTIES FROM THE PREDICTED ARRIVING WIND

Existing SHOLs are derived mainly for manned aircraft tend to focus upon the short term mean wind arriving at a vessel. Hence the bare prediction process described in section 3 is adequate for such applications. In fact very little extra is required for air recovery of all types of air-vehicle on the bow mounted landing pads common in offshore service vessels. However as indicated in the introduction the flight-deck in many military craft is often located aft were recovery is strongly affected by the turbulent air-wake created by the superstructure. Furthermore, because UAVs typically have less penetration into aggressive airflows than their larger manned counterparts the provision of more detailed air-wake information to UAV flight controllers during recovery would be highly beneficial.

Given that the air-wake flows encountered during recovery are chaotic in nature it is only possible to consider their short-term statistical properties. Clearly these properties will scale with the wind speed and be affected by the vessel heading relative to the mean wind direction where for most recovery operations the preferred vessel course is to produce head or near head winds.

#### 2.3.1 LiDAR-based sea trial

In order to explore typical relationships between the incoming wind and the flight deck flows a sea trial was conducted in 2019 aboard a Tide Class Royal Fleet

 ©2021: The Royal Institution of Naval Architects

Auxiliary tanker with a helicopter flight deck located at the stern. The arrangement was as shown in Figure 1 with a long-range Doppler LiDAR mounted just aft of the bow and short range LiDARs that exhibit high spatial resolution mounted on the flight deck pointing vertically upward. The detailed specifications and the instruments employed are given in section 2.3.2. In order to allow the LiDAR beam scan angle to be compensated for vessel motion the craft was fitted with a high resolution 6 degree of freedom motion sensor.

Examples of the key experimental findings are presented in Figures 3 and 4. Figures 3a-c show the predicted wind arriving at the vessel using the time evolving advection technique and subsequently measured winds arriving at the vessel as a function of predict ahead time the maximum value of which was 180 seconds. It should be noted that as shown in the legends the symbols used in Figure 3a to denote the predicted and measured wind are the reverse to those in Figures 3b and 3c.

The vessel was nominally steering into wind however to obtain a better estimate of the actual relative wind and hence the true component advecting towards the vessel the LiDAR beam was scanned in an angular fan. The maximum wind value was then estimated by taking the largest 8 values of speed verses angle and least squares fitting these to a quadratic angular dependence model. The maximum value was then computed from the best fit model.  Only 8 values were used for two reasons, firstly because the quadratic model was clearly only a second order Taylor expansion of the projected cosine value of the true wind onto the beam direction and secondly to minimise the temporal smearing due to the finite time required to execute the angular fan of scans.

A more detailed time local view of the predictions is shown in Figure 4.

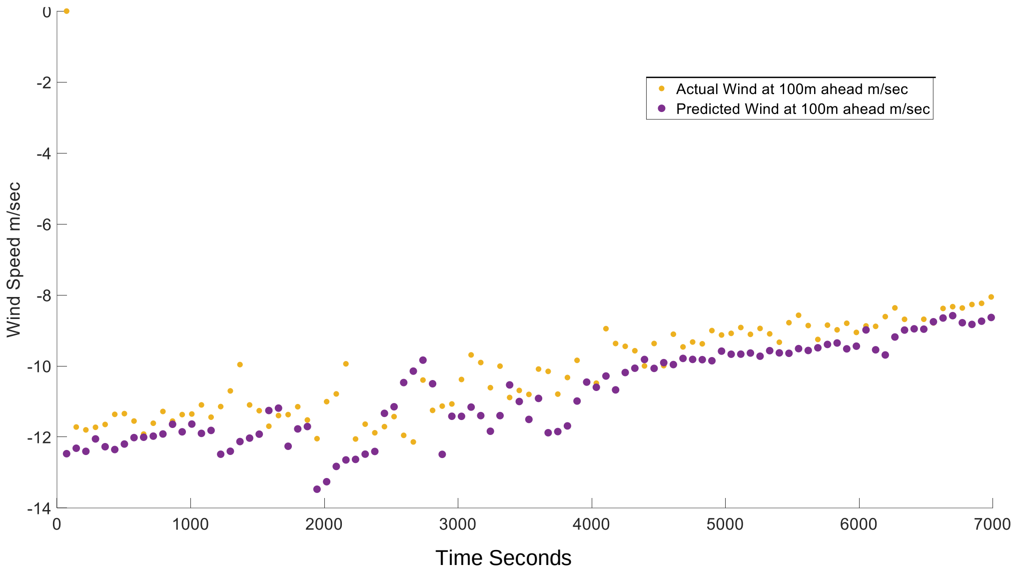


Figure 3a: Comparison of 60 sec ahead predicted and measured winds arriving at the vessel.

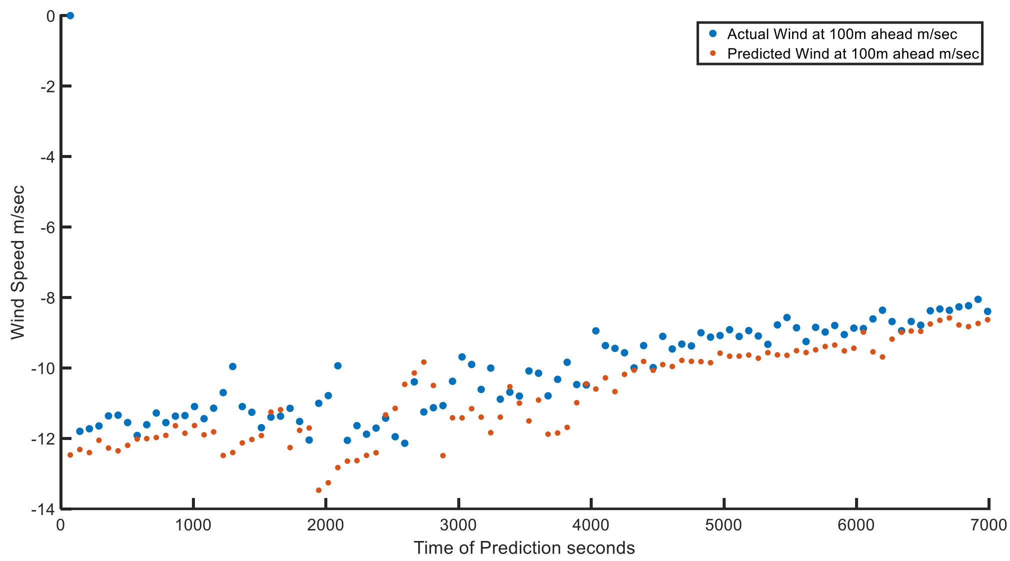


Figure 3b: Comparison of 120 sec ahead predicted and measured winds arriving at the vessel.

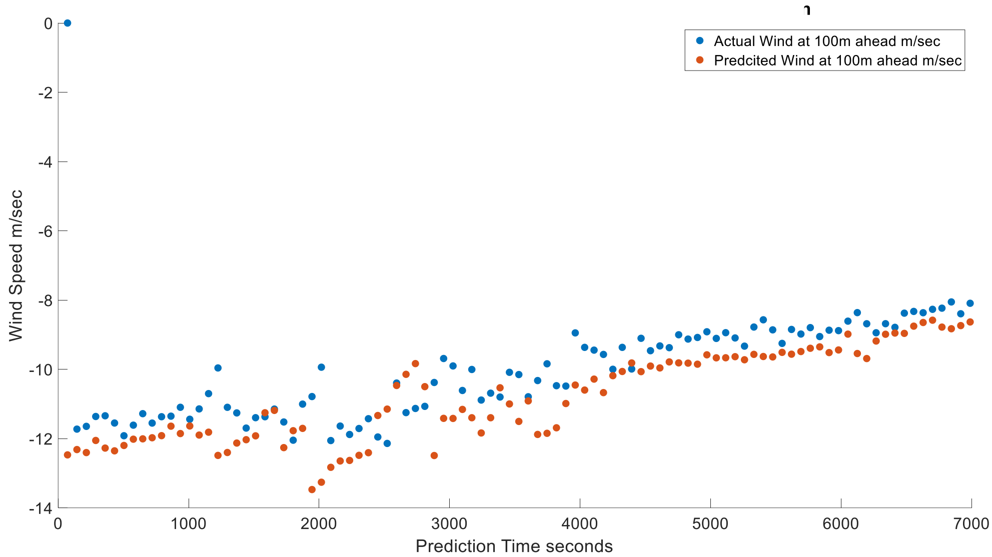


Figure 3c: Comparison of 180 sec ahead predicted and measured winds arriving at the vessel.


©2021: The Royal Institution of Naval Architects

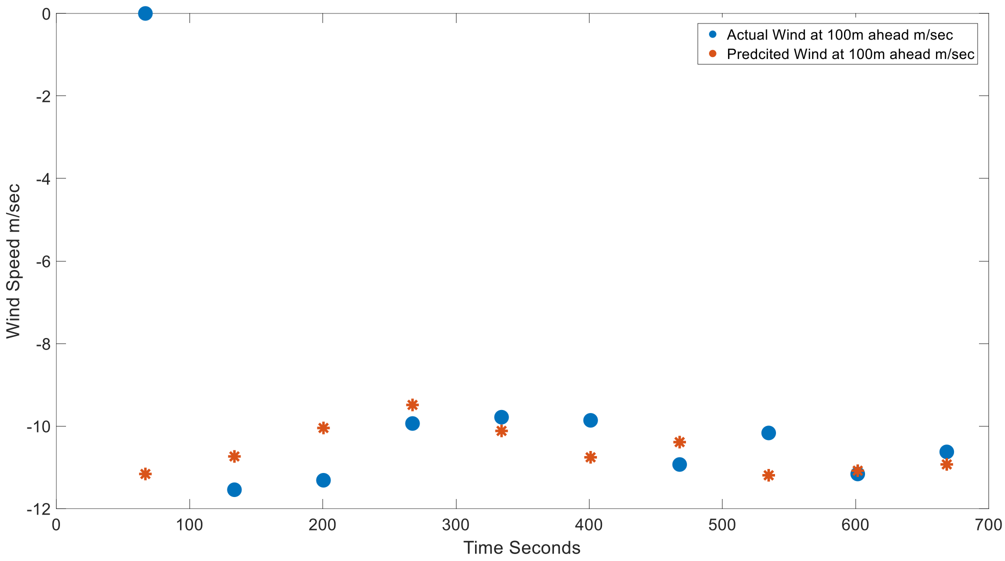


Figure 4: A short timescale comparison of 60 sec ahead predicted and measured winds arriving at the vessel. The first blue point is artificial for scaling purposes.

The flow properties observed at different heights over the flight deck are shown in Figure 5 together with the corresponding predicted arriving wind strength. In order to relate the results more directly to the level of aerodynamic forces acting on an air vehicle the squares of the various properties are plotted.

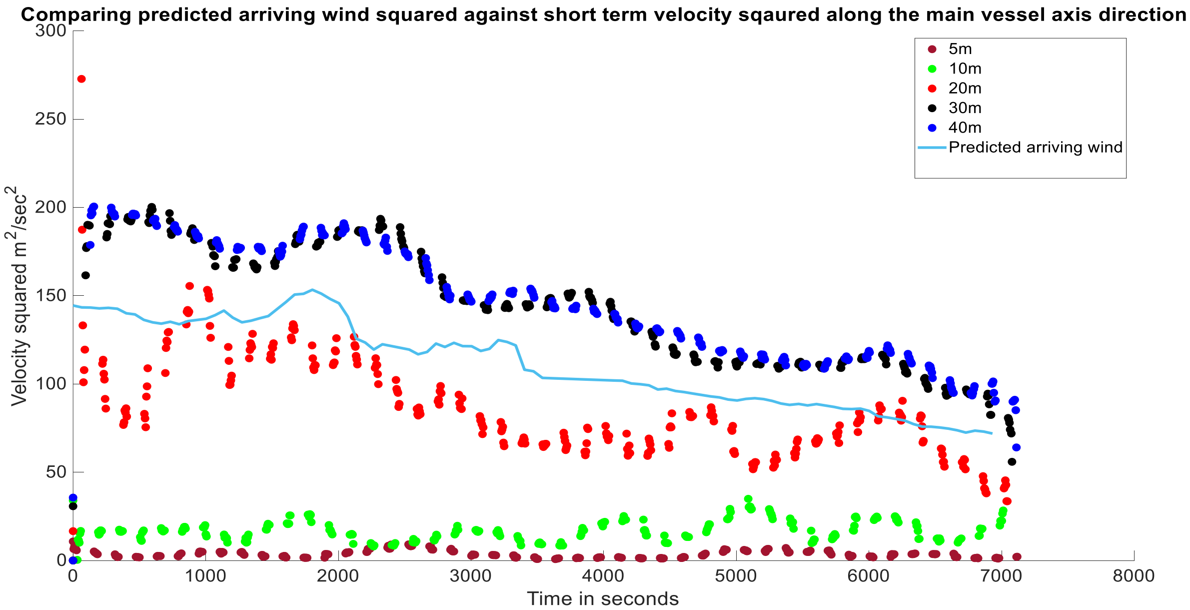


Figure 5: Comparison of the square of the predicted arriving wind with the short-term averaged velocity squared values over the flight deck in the main vessel axis direction. The predicted arriving wind is the solid line.

The superstructure of the vessel extended to approximately 20m above deck height. The results follow the expected behaviour in that both the mean level and the scale of the fluctuations of the airflow over the flight deck follow closely the predicted arriving wind at the vessel. Thus, the predictions drawn from the long-range LiDAR measurements are reliably able to track the short-term statistical properties of the flight deck airflow.

The forward-facing LiDAR beam was set below the level of the stern superstructure and thus as expected the relatively steady flow at 40m corresponding to the free stream over the vessel and is larger than the arriving flow. As the elevation above deck reduces the ratio of the mean to the fluctuating flow decreases down low values at deck level where the flow is essentially noise-like. From a recovery perspective the most critical region is where the UAV transitions from the free stream to the chaotic flows behind the superstructure. The data shows that the trends in the flow properties at this transition height are well described by the predicted wind arriving at the vessel. Telemetering such information to the flight controller of a UAV would significantly aid in its recovery approach, particularly as UAVs evolve to having greater and greater autonomy.

### 2.3.2 LiDAR system specifications

The forward-facing long-range LiDAR was a Halo Photonics Ltd., “Stream Line” device. This was a pulsed Doppler LiDAR which recorded the component of the prevailing wind speed along the beam line. Typically, 1500 spatial samples were recorded along the beam direction out to ranges of up to several km (the exact range being dependent upon aerosol density). The spatial samples were obtained during the transit time of LiDAR light out to full range and return and hence in the present context can be considered to be instantaneous. The instruments could be operate at a maximum repetition cycle rate of 10Hz, i.e., a set of 1500 spatial samples every 0.1 sec. The instrument was equipped with a three-dimensional scanner allowing it in principle to explore a full upper hemisphere, however in the sea trial the beam was scanned in a flat fan of 15 separate lines at deck level. As with all measurements of the present type the sample variance was an inverse function of the aperture time. The results shown in Figure 2 were obtained from scans over a periodic arc (typically $-20^\circ \rightarrow +20^\circ$ the vessel centre line) executed during 15 seconds. The length of the light pulse employed produced an effective spatial resolution of approximately 30m which was adequate for the forward measurements.

It is possible to increase the spatial resolution of this type of pulsed Doppler LiDAR if fine detail of close in winds are required. This is accomplished by forcing the light pulses employed to deliberately overlap. This produces a superimposed set of overlapping convolutions of the wind data (at a significantly higher resolution than otherwise possible) with the Gaussian profile of the LiDAR pulse. By knowing the profile of the pulse and employing deconvolution techniques, it is possible to estimate the original wind data at significantly higher spatial resolution, (Gurdev et al 1996, Belmont et al 2017). Using this technique, it has been possible to increase the spatial resolution by 3 to 5 times depending on the prevailing signal to noise ration present in the raw LiDAR wind measurements.

The two short range Doppler LiDARs were mounted along the vessels centre line on the flight deck. One was at the touchdown point and one approximately 5m from the stern. These were continuous beam devices as opposed to the pulsed variant used for the forward measurements. These instruments were “Wind Scout” instruments produced by METEK SA. They deliver fully vector resolved wind measurements by scanning around a small disk-shaped region. Hence such devices measure vertically but unlike the pulsed LiDARs return a full vector wind velocity rather than the component along the beam direction. The spatial resolution varied from 0.1m at 2m above the flight-deck level to 2m at 40m. These devices produced a vector wind value at a rate of 1 Hz.

## 2.4 AN ARTIFICIAL INTELLIGENCE ENHANCED RECOVERY TOOL

As indicated in section 1 the first implementation of an air-wake prediction-based recovery advice system would simply need to predict the intensity of the arriving wind. This is essentially a SHOL based prediction approach.

To move to more sophisticated systems able to provide a UAV flight controller with more detailed information for aiding recovery a system is required that associates the predicted arriving wind with either the corresponding expected flight deck flows or with the anticipated ease of recovery for the specific UAV. This is the role of the classifier which is an artificial intelligence system that identifies and classifies the characteristics of the incoming airflow and then identifies the most probable corresponding match in a database of flight deck airflow properties. Clearly the classifier will need to have knowledge of the impact of the class of predicted arriving wind on recovery of a given air-vehicle type on a given class of vessel. Here the term class of wind conditions would be expected to be set by the directional power density spectrum of the wind.

Such a system would be initially loaded with previously acquired information about the relationships between the flight deck flows and the arriving winds. Such initial data would be obtained from a variety of sources such as field trials of the type described here and from off-line CFD simulations. Once operational the AI system will grow in capability over time by continuously updating the databases for the results of actual recovery operations. This learning process can be considerably accelerated if the updating process takes place across all the vessels in each type exchanging data-base information. Ideally the

 ©2021: The Royal Institution of Naval Architects

flight deck would be equipped with upward pointing short range Doppler LiDAR to log the actual airflows, however in the absence of this the flight logs recorded by both UAVs and manned aircraft during each recovery will provide “quality of recovery” information that can be incorporated into the data base. The AI system would thus need to be capable of associating the predicted wind arriving at the vessel with various different types of information, ranging from explicit flow properties to more metric like parameters such as quality measures of the ease of recovery.

## 3. CONCLUSIONS

The authors have demonstrated the capability of the forward prediction of the properties of the arriving wind at a vessel for time intervals adequate to significantly aid in the recovery of a wide range of air vehicles onto vessels. For craft with flight decks sited in the fore part of the vessel it is adequate to simply predict the arriving wind. For the more difficult task of recovery to stern areas behind superstructure it is also necessary to predict either the explicit properties of the turbulent air-wake or else to predict some quality measure for the aid of recovery under the prevailing conditions. As would be anticipated it has been confirmed that the trends in the properties of flight deck and hence of recovery quality measures follow the trends in the predicted arriving wind.

## 4. ACKNOWLEDGEMENTS

The authors would like to acknowledge the support of the UK Ministry of Defence in resourcing the sea trial which provided the data upon which this work was based.

## 5. REFERENCES


1. BANAKH, V. A., and SMALIKHO I. N. (1997). *Estimation of turbulent energy dissipation rate from data of pulse Doppler lidar*. Atmos. Oceanic Opt., 10, 957–965.
2. BELMONT M. R., CHRISTMAS J., DUNCAN J. M., DUNCAN J., and FERRIER B. (2017). *Real-time ship air-wake and freee stream measurements using Doppler LiDAR*. Int. Conf., on Computer Applications in Shipbuilding, Sept 26-28, Singapore.
3. DAVIES, F., COLLIER C. G., PEARSON G. N., and BOZIER K. E. (2004). *Doppler Lidar measurements of turbulent structure function over an urban area*. J. Atmos. Oceanic Technol., 21, 753–761.
4. DROBINSKI, P., Brown R. A., FLAMANT, P. H., and PELON J. (2004). *Evidence of organized large eddies by ground-based Doppler Lidar, sonic anemometer and sodar*. Bound.-Layer Meteor., 88, 343–361.
5. FRISCH U. (1995). *Turbulence, The Legacy of A. N. Kolmogorov*. Cambridge University Press, Cambridge. 296 pp. ISBN 0 521 45713.
6. GURDEV L. L., DREISCHUH T. N., and STYANOV D. V. (1996). *De-convolution algorithms for improving the resolution of exponential-shaped pulse lidars*. Proc. of the Ninth International School on Quantum Electronics: Lasers-Physics and Applications. SPIE vol 3052, pp 310-315.
7. HUANG N. E., SHEN Z., LONG S.R., WU M.C., SHIH H.H., ZHENG Q., YEN N.C., TUNG C.C., LIU H.H. (1971). *The Empirical Mode Decomposition and the Hilbert Spectrum for Nonlinear and Nonstationary Time Series Analysis*. Proceedings of the Royal Society of London A. **454** (1971): 903–995.
8. LIU, Z., BARLOW, J. F., CHAN, P.-W., FUNG, J. C. H., LI, Y., REN, C., MAK, H. W. L. and NG, E. (2019) *A review of progress and applications of pulsed doppler wind LiDARs.* Remote Sensing, 11 (21). 2522. ISSN 2072-4292.
9. O’CONNOR E. J., ILLINGWORTH A. J., BROOKS I. M., WESTBROOK C. D., HOGAN R. J., DAVIES F., and BROOKS B. J. (2010). *A method for estimating the turbulent kinetic energy dissipation rate from a vertically-pointing Doppler lidar, and independent evaluation from balloon-borne in-situ measurements.* Journal of Atmospheric and Oceanic Technology, vol. 27, pp 1652-1664.
10. SREENIVASAN K. R., and ANTONIA R. A. (1997). *The phenomenology of small-scale turbulence*. Annu. Rev. Fluid Mech. 29, 435.
11. TAYLOR G. I. (1938). *The Spectrum of Turbulence*. Proc. R. Soc. London, Ser. A 164, 476.


©2021: The Royal Institution of Naval Architects 

**APPENDIX 1: MORE SOPHISTICATED ADVECTION**

A LINEAR FIRST ORDER LOCAL VELOCITY MODEL

A space/time model of the local velocity, $V(x,\tau)$, along the LiDAR beam line is determined by fitting a polynomial function to the LiDAR data. This is the component in the direction of the maximum wind local velocity as determined from an angular fan of LiDAR measurements. The simplest extension of the constant velocity "Magic Carpeting" approach is to model the local wind velocity, $V(x,\tau)$, by a first order spatio-temporal polynomial:

$$V(x,\tau)=a_0+a_1x+a_2\tau+a_3x\tau \qquad \text{1A}$$

It is assumed that this direction which corresponds to the direction of maximum velocity does not change over the short timescale of interest. This first order model will be extended in section A2 to include higher order corrections using perturbation methods.

The, $x$, location of the point where prediction is required at time, $t$, from the start of the set of LiDAR scans used is determined by a combination of the chosen starting location, $x_0$, along the LiDAR beam line and the total distance, $s(t)$, travelled along the trajectory determined by, $V(x,\tau)$, during the elapsed time, $t$. At the instant, $\tau$:

$$x=x_0-s(\tau) \qquad \text{2A}$$

During the time interval, $\tau\rightarrow\tau+d\tau$, the distance travelled changes by, $ds$, where:

$$ds=V(x,\tau)d\tau \qquad \text{3A}$$

Hence the total distance travelled, $s(t)$, during time, $t$, is given by:

$$s(t)=\int_{\tau=0}^{t}V(x_0-s(\tau),\tau)d\tau \qquad \text{4A}$$

Substituting from 1A into 4A gives:

$$s(t)=\int_{\tau=0}^{t}\left\{a_0+a_1(x_0-s(\tau))+a_2\tau+a_3(x_0-s(\tau))\tau\right\}d\tau \qquad \text{5A}$$

Differentiating equation 5A w.r.t, $t$, gives:

$$\frac{ds(t)}{dt}+s(\tau)\{a_1+a_3t\}=a_0+a_1x_0+(a_2+a_3x_0)t \qquad \text{6A}$$

The solution to equation 6A is:

$$s(t)=e^{-\int_t\{a_0+a_3\lambda\}d\lambda}\left[\int_t e^{-\int_\lambda\{a_0+a_3\varepsilon\}d\varepsilon}\left\{a_0+a_1x_0+(a_2+a_3x_0)\lambda\right\}d\lambda+C\right] \qquad \text{7A}$$

Thus the detailed wind structure measured by the LiDAR in a local region around, $x_0$, of the wind system starting at, $t=0$, will have propagated in time, $t$, to the location, $x=x_0-s(t)$. Partial evaluation of equation 7A gives:

$$s(t)=e^{-\left\{a_0t+a_3\frac{t^2}{2}\right\}}\left[\int_t e^{\left\{a_0\lambda+a_3\frac{\lambda^2}{2}\right\}}\left\{a_0+a_1x_0+(a_2+a_3x_0)\lambda\right\}d\lambda+C\right] \qquad \text{8A}$$

Evaluation of the remaining integrals in equation 8A produces after the determination of the constant, $C$, (required to satisfy the initial condition, $t=0$, $s(0)=0$):

$$s(t)=$$

$$\frac{1}{2(-a_3)^{\frac{3}{2}}}\left[\sqrt{2\pi}\left(a_0a_3-a_1a_2\right)\left\{e^{\frac{-(a_1+a_3t)^2}{2a_3}}erf\left(\frac{(a_1+a_3t)}{\sqrt{-2a_3}}\right)-e^{-\frac{a_1^2}{2a_3}}erf\left(\frac{a_1}{\sqrt{-2a_3}}\right)\right\}\right] \qquad \text{9A}$$

Hence using equations 2A and 9A the, $x$ coordinate, $x(t)$ of the advected point starting at, $x_0, t=0$, is:

$$x(t)=$$

$$x_0-\frac{1}{2(-a_3)^{\frac{3}{2}}}\left[\sqrt{2\pi}\left(a_0a_3-a_1a_2\right)\left\{e^{\frac{-(a_1+a_3t)^2}{2a_3}}erf\left(\frac{(a_1+a_3t)}{\sqrt{-2a_3}}\right)-e^{-\frac{a_1^2}{2a_3}}erf\left(\frac{a_1}{\sqrt{-2a_3}}\right)\right\}\right] \qquad \text{10A}$$

 ©2021: The Royal Institution of Naval Architects

A QUADRATIC HIGHER ORDER LOCAL VELOCITY MODEL

The description in the previous section employed a model that described the local velocity in terms of linear variations in space and time. If the data suggests it is appropriate to introduce additional modest higher order corrections a perturbation scheme is the natural approach. In order to illustrate the methodology small quadratic spatial and temporal terms will be incorporated. The local velocity model given in equation 1 is then relabelled as, $V_0(x,\tau)$, and the new higher order model, $V(x,\tau)$, is written in the form:

$$V(x,\tau)=V_0(x,\tau)+\varepsilon\{a_4x^2+a_5\tau^2\}\qquad 11A$$

where, $\varepsilon$, is a small scaling parameter which ensures that the two extra terms, $\varepsilon a_4x^2$, and, $\varepsilon a_5\tau^2$, are small corrections to, $V_0(x,\tau)$. The actual coefficient values obtained from fitting the polynomial to the LiDAR data for the new, $x^2$, and, $\tau^2$, terms being respectively, $\varepsilon a_4$, and, $\varepsilon a_5$. There is no requirement to add in an, $x\tau$, term as that was already present in, $V_0(x,\tau)$.

In such a perturbation approach it is assumed that the new terms produce a modest change, $\varepsilon s_1(\tau)$, in the original solution. Relabelling this original solution as, $s_0(\tau)$, gives:

$$s(\tau)=s_0(\tau)+\varepsilon s_1(\tau)\qquad 12A$$

The perturbed form of equation 6 then becomes:

$$s_0(t)+\varepsilon s_1(t)=\int_{\tau=0}^{t}\Big[a_0+a_1\{x_0-s_0(\tau)-\varepsilon s_1(\tau)\}+a_2\tau+a_3\{x_0-s_0(\tau)-\varepsilon s_1(\tau)\}\tau$$
$$+\varepsilon a_4\{x_0-s_0(\tau)-\varepsilon s_1(\tau)\}^2+\varepsilon a_5\tau^2\Big]d\tau\qquad 13A$$

Expanding out equation 13A and retaining only terms up to order, $\varepsilon$, produces:

$$s_0(t_{total})+\varepsilon s_1(t_{total})=\int_{\tau=0}^{t_{total}}\Big[a_0+a_1x_0+a_2\tau+a_3x_0\tau-a_1s_0(\tau)-a_3s_0(\tau)\tau$$
$$-\varepsilon\left\{a_1s_1(\tau)+a_3s_1(\tau)\tau-a_4\left(x_0-s_0(\tau)\right)^2-a_5\tau^2\right\}\Big]d\tau\qquad 14A$$

Applying equation 6 (which now represents the, $s_0(\tau)$, equation) to 14A gives:

$$s_1(t)=\int_{\tau=0}^{t}\Big[a_1s_1(\tau)+a_3s_1(\tau)\tau-a_4\left(x_0-s_0(\tau)\right)^2+a_5\tau^2\Big]d\tau\qquad 15A$$

which has the same form as equation 5A producing the same class of inhomogeneous first order ordinary differential equation as equation 6A, i.e.:

$$\frac{ds_1(t)}{dt}+s_1(t)\{a_1+a_3t\}=a_4\left(x_0-s_0(t)\right)^2+a_5t^2\qquad 16A$$

Equation 16A has the solution:

$$s_1(t)=e^{-\left\{a_0t+a_3\frac{t^2}{2}\right\}}\left[\int^{t}e^{\left\{a_0\lambda+a_3\frac{\lambda^2}{2}\right\}}\left\{a_4\left(x_0-s_0(\lambda)\right)^2+a_5\lambda^2\right\}d\lambda+C_1\right]\qquad 17A$$

whereas with equation 8A the constant, $C_1$, is evaluated to satisfy the initial condition, $s_1(0)=0$.The term, $\left(x_0-s_0(\lambda)\right)^2$, means that the integral in equation 17A cannot be expressed in terms of elementary functions, however it can be efficiently evaluated numerically or alternatively given the very gentle curvature of, $s_0(t)$, the term, $\left(x_0-s_0(\lambda)\right)^2$, can be fitted to a low order polynomial which will in general yield a closed form integral. Given the potentially "stiff" nature of the exponential factors in equation 17A either approach is preferable to a direct numerical solution of the differential equation.